Journal of Applied Physics

Heat exchange with interband tunneling

Cite as: J. Appl. Phys. **126**, 165107 (2019); https://doi.org/10.1063/1.5113870
Submitted: 11 June 2019 • Accepted: 08 October 2019 • Published Online: 24 October 2019

Zheng Li, Jin Xue and Rajeev J. Ram

Journal of Applied Physics ARTICLE scitation.org/journal/jap

Heat exchange with interband tunneling

Cite as: J. Appl. Phys. **126**, 165107 (2019); doi: 10.1063/1.5113870
Submitted: 11 June 2019 · Accepted: 8 October 2019 ·
Published Online: 24 October 2019

Zheng Li,[a] Jin Xue, and Rajeev J. Ram

AFFILIATIONS

Research Laboratory of Electronics, Massachusetts Institute of Technology, Cambridge, Massachusetts 02139, USA

[a]zhli@mit.edu

ABSTRACT

The carrier transport associated with interband tunneling in semiconductors has been investigated extensively both experimentally and theoretically. However, the associated heat exchange from interband tunneling is not discussed in depth. Due to the nanoscale nature of the tunneling phenomenon, people tend to use a "resistor model" to compute the heat generated. We present our analysis of heat exchange in tunneling junctions based on an extended Kane's model. We observe that the heat exchange is distinct when we apply forward bias, small reverse bias, and large reverse bias. In each of these bias regimes, we demonstrate that the internal temperature distribution of a tunneling junction can deviate from the simplified "resistor model" significantly.

I. INTRODUCTION

Interband tunneling has been extensively studied for more than half a century since the proposal of the Zener breakdown mechanism[1] and the subsequent invention of Esaki diodes.[2] Although the interband tunneling effect is also responsible for unwanted contributions to the gate-induced drain leakage in metal-oxide-semiconductor field-effect transistors (MOSFETs)[3] and parasitic dark currents in photodetectors,[4] the associated effect of negative differential resistance exhibited in forward-biased Esaki diodes has given rise to a number of useful devices including high-frequency oscillators, amplifiers, and switches.[5] More recently, interband tunneling field-effect transistors (TFETs) based on both traditional bulk semiconductors and novel 2D/nanostructured configurations have been proposed as a promising alternative to MOSFETs for further down-scaling of the transistor power supply voltage and more energy-efficient switching capability.[6–8] This is fundamentally due to the benefit of interband tunneling for the "cold" carrier injection in TFETs, instead of the thermal injection associated with a Boltzmann tail in MOSFETs which is ultimately subject to the 60 mV/dec limit of the subthreshold swing at room temperature.

Models of charge transport within semiconductor interband tunneling devices successfully predict device electrical characteristics.[9–19] However, the associated thermal transport has not received equal attention, and tunnel diodes are traditionally treated simply as lumped resistive-heating elements. In contrast, bipolar thermoelectric effects in semiconductor diodes in the diffusive transport regime are now well established.[20–22] Similarly, the local heating/cooling effects associated with quantum mechanical tunneling processes in other (unipolar) devices such as field emission structures,[23,24] metal-insulator-metal junctions,[25] metal-insulator-superconductor junctions,[26,27] and magnetic tunnel junctions[28,29] have also been investigated.

In this letter, we model the heat exchange in tunneling diodes based on direct bandgap materials and compute the associated internal temperature profiles. We present the extended Kane's model and use it to compute the current density and the associated heat exchange. By assuming a varying energy relaxation length and simulating the internal temperature profiles using Fourier's law, we conclude that our results deviate significantly from the "resistor model" when the electron energy relaxation length is comparable to the length of the n bulk region. Our model also predicts that cooling should be observed with small reverse bias.

II. DIRECT BAND-TO-BAND TUNNELING MODELS

By using perturbation theory with the two-band $k \cdot p$ Hamiltonian, Kane derived the transmission probability and the current density of direct interband tunneling under a constant electrical field F.[9,10] The band structure and some related parameters are present in Fig. 1. Note here that the constant field is the average electrical field in an abrupt pn junction.

Although the two-band Kane's model qualitatively captures the IV characteristics of a tunneling junction, the simulated current density can deviate from that of the quantum simulations[17,30–33] since Kane's two-band model does not incorporate multiband mixing and nonparabolicity when k is large. After Kane, Krieger also

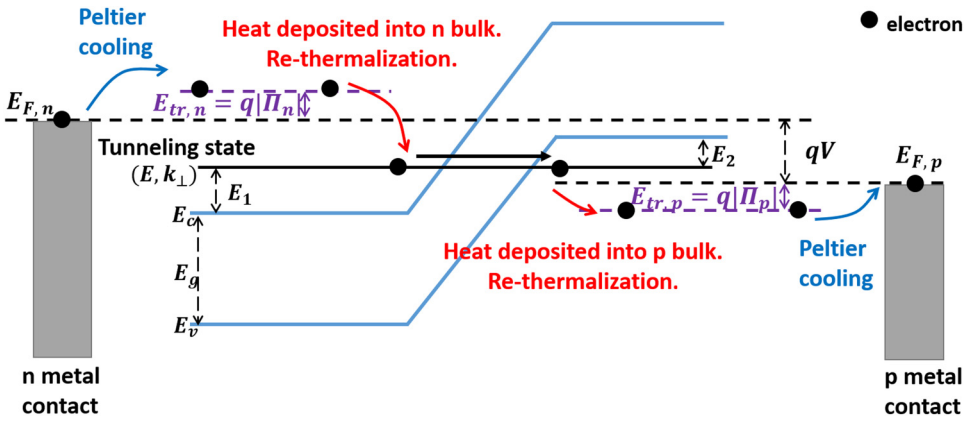

FIG. 1. The band structure and the associated electrical and thermal transport processes of a forward-biased junction. The solid blue lines indicate the band structure. The dashed black lines indicate the Fermi levels. The solid black line indicates a tunneling state labeled with $(E, k_\perp)$. The dashed purple lines indicate the transport energy in the bulk. E_1 and E_2 are the kinetic energy of the state in the conduction band and the valence band, respectively.

considered junctions with constant fields and computed the tunneling transmission probability by using a four-band Hamiltonian and treating the effect of the remote bands as perturbation.[34] Recently, Pan *et al.* used Krieger's multiband model without considering the perturbation from remote bands to simulate the tunneling current in bulk and low-dimensional materials.[17,35] They also compared their results using full quantum transport simulations with nonequilibrium Green's function (NEGF)[36] and found that the tunneling current density was consistent for various III-V materials and in a relatively wide range of field strength. Louran *et al.* also modeled GaAs tunnel junctions using similar multiband corrections and found reasonable agreement with NEGF methods and experiments.[37]

In Fig. 1, according to Krieger's work,[34] given the bandgap E_g, the constant field F, the spin–orbit coupling strength Δ, and the transition dipole strength P, the transmission probability T_{4b} of an electron with energy E and transverse wavevector $k_\perp$ is

$$T_{4b}(E, k_\perp) = \frac{\pi^2}{9}\exp\left(-\frac{\pi E_g^2}{4qFP}\sqrt{\frac{3+6\alpha}{3+4\alpha}}\left(1+\frac{4P^2k_\perp^2}{E_g^2}\right)\right), \quad (1)$$

where $\alpha = \frac{\Delta}{E_g}$.

The current density can be evaluated

$$\begin{aligned} J_{4b} &= \frac{q}{\pi\hbar}\int dE\left[f_n(E) - f_p(E)\right]\int \frac{dk_\perp^2}{(2\pi)^2}T_{4b}(E, k_\perp) \\ &= A_{4b}(F)\exp\left(-\frac{B_{4b}}{F}\right) \\ &\quad\times\int dE\left[f_n(E) - f_p(E)\right](1 - R_{4b}(E, F)), \end{aligned} \quad (2)$$

with A_{4b}, B_{4b}, and R_{4b} being defined as

$$B_{4b} = \frac{\pi m_r^{\frac{1}{2}}E_g^{\frac{3}{2}}}{2q\hbar}\sqrt{\left(\frac{(5+4\alpha)(1+2\alpha)}{(2+2\alpha)(3+4\alpha)}\right)}, \quad (3a)$$

$$A_{4b}(F) = \frac{q^2B_{4b}F}{9\pi^2\hbar E_g^2} + \frac{q^2F^2}{18\pi^2\hbar E_g^2}, \quad (3b)$$

$$R_{4b}(E, F) = \exp\left(-\frac{6+6\alpha}{5+4\alpha}\frac{B_{4b}}{m_rFE_g}\min(2m_cE_1, 2m_{lh}E_2)\right). \quad (3c)$$

Here, $f_{n,p}$ are the Fermi-Dirac distributions in the n and p bulk. E_1 and E_2 are the kinetic energy of the tunneling electron in the conduction band (CB) and the light hole valence band (LH-VB), respectively (see Fig. 1). m_r is the reduced mass of the conduction band (CB) and the light hole valence band (LH-VB) effective mass m_c and m_{lh},

$$m_r = \left(\frac{1}{m_c} + \frac{1}{m_{lh}}\right)^{-1}. \quad (4)$$

Note that the factor $1 - R_{4b}$ is from the upper limit of the integral over $k_\perp$,

$$\hbar^2k_\perp^2 < \min(2m_cE_1, 2m_{lh}E_2). \quad (5)$$

In Fig. 2, we present the comparison of the $J - V$ curves of tunneling junctions based on direct and low bandgap semiconductor $In_{0.53}Ga_{0.47}As$ using the two-band and the four-band Kane's models. At each bias, we use the average electrical field in the abrupt pn junctions as F in Eq. (2). Some related parameters are present in Table I. InGaAs is chosen for its efficient junction tunneling with an abrupt high doping profile and also for its low thermal conductivity and thus more conspicuous internal heating effects. We observe that the current density from the four-band Kane's model is always higher. This is consistent with the work of Pan *et al.*[17] We will use the four-band Kane's model in our following discussions.

III. INTERFACIAL HEAT EXCHANGE

The tunneling current causes heat exchange near the bulk/barrier interfaces due to the difference between the average tunneling

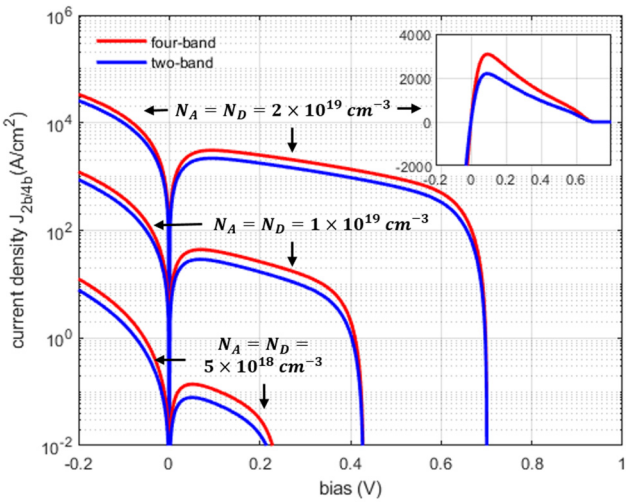

FIG. 2. The current density vs the bias of InGaAs tunneling junctions with a multiple doping level. The blue lines and the red lines indicate the results from the two-band and the four-band Kane's models, respectively. The curves of $N_A = N_D = 2 \times 10^{19}$ in a linear scale are present in the inset plot.

electron energy and the average transport energy in the bulk. The main heat exchange processes near the junction are depicted in Fig. 1. Here, we assume that the energy-relaxation processes only occur in the n/p bulk regions since the barrier region (<20 nm) is short and the tunneling process can be considered ballistic. In the bulk region, the heat exchange takes place approximately within an energy relaxation length from the junction. In the n bulk, the scattering between the electrons in the CB and the optical phonons dominates, and the energy relaxation length l_n is on the order of several hundred nanometers for most III-V materials.[38,39] In the p bulk, the energy relaxation length l_p tends to be much smaller than l_n because holes relax faster than electrons through the carrier-optical phonon scattering[40–43] and have a lower velocity for both drift and diffusion processes due to the larger effective mass.

We can compute the average transport energy referred to the Fermi level in the bulk as

$$E_{tr,n/p} = q|\Pi_{n/p}|, \tag{6}$$

TABLE I. Parameters of InGaAs in our simulations.

Parameters	Values
E_g	0.74 eV
Δ	0.329 eV
m_c	0.041 m_0
m_{lh}	0.052 m_0
Dielectric constant ϵ	13.9061
Thermal conductivity κ	0.05 W cm^{-1} K^{-1}

where $\Pi_{n/p}$ is the Peltier coefficient in the n/p bulk.[44] Under the relaxation-time approximation,[20,45,46]

$$\Pi_n \approx -\frac{1}{q}\frac{\int \tau_n(E)\overline{v_{x,n}}^2(E)DOS_n(E)(E-E_F)\left(-\frac{\partial f_n}{\partial E}dE\right)}{\int \tau_n(E)\overline{v_{x,n}}^2(E)DOS_n(E)\left(-\frac{\partial f_n}{\partial E}dE\right)}, \tag{7a}$$

$$\Pi_p \approx \frac{1}{q}\frac{\int \tau_p(E)\overline{v_{x,p}}^2(E)DOS_p(E)(E-E_F)\left(-\frac{\partial f_p}{\partial E}dE\right)}{\int \tau_p(E)\overline{v_{x,p}}^2(E)DOS_p(E)\left(-\frac{\partial f_p}{\partial E}dE\right)}, \tag{7b}$$

where $f_{n/p}$ is the Fermi-Dirac distribution function, $\tau_{n/p}(E)$ is the carrier energy relaxation time, $\overline{v_{x,n/p}}(E)$ is the averaged carrier velocity, and $DOS_{n/p}(E)$ is the density of states. Approximately,

$$\tau_{n/p}(E) \propto |E - E_{c/v}|^{r-\frac{1}{2}}, \tag{8}$$

where r is a scattering parameter associated with the detailed energy relaxation mechanisms.

In our model, an energy-indepedent relaxation time, or $r = \frac{1}{2}$, is used. This is consistent with the fact that the electron-polar optical phonon (POP) scattering dominates the energy relaxation for III-V semiconductors at room temperature.[47] Also, in Eqs. (7a) and (7b), the integration is essentially only within a window of kT near the Fermi levels, and thus, we do not expect the relaxation time to vary significantly with energy.

Assuming parabolic conduction and valence bands, Eqs. (7a) and (7b) can be further simplified as

$$\Pi_n \approx -\frac{1}{q}\frac{\int (E-E_c)^{\frac{3}{2}}(E-E_F)\left(-\frac{\partial f_n}{\partial E}dE\right)}{\int (E-E_c)^{\frac{3}{2}}\left(-\frac{\partial f_n}{\partial E}dE\right)}, \tag{9a}$$

$$\Pi_p \approx \frac{1}{q}\frac{\int (E_v-E)^{\frac{3}{2}}(E-E_F)\left(-\frac{\partial f_p}{\partial E}dE\right)}{\int (E_v-E)^{\frac{3}{2}}\left(-\frac{\partial f_p}{\partial E}dE\right)}. \tag{9b}$$

We can define the average energy of the tunneling electrons as

$$E_{Q,n/p} = \frac{1}{J_{4b}}\int dE(E - E_{F,n/p})\frac{\partial J_{4b}}{\partial E}. \tag{10}$$

Note that E_F here as the reference energy can be either $E_{F,n}$ or $E_{F,p}$, depending on which bulk we discuss. In our following discussion, we will use E_Q for the energy level and $E_{Q,n/p}$ for E_Q referred at $E_{F,n/p}$.

The heat exchange Q_n and Q_p in the n and p bulks can be expressed as

$$Q_n = \frac{1}{q}\int dE(q|\Pi_n| - (E - E_{F,n}))\frac{\partial J_{4b}}{\partial E} = \frac{1}{q}J_{4b}(q|\Pi_n| - E_{Q,n}), \tag{11a}$$

$$Q_p = \frac{1}{q}\int dE((E - E_{F,p}) - q|\Pi_p|)\frac{\partial J_{4b}}{\partial E} = \frac{1}{q}J_{4b}(E_{Q,p} - q|\Pi_p|). \quad (11b)$$

It is expected that the heat exchange is the product of the carrier flux J_{4b}/q and the heat exchanged per carrier, which are $q|\Pi_n| - E_{Q,n}$ and $E_{Q,p} - q|\Pi_n|$ for n and p bulks, respectively.

In Figs. 3(a) and 3(b), we plot the heat flux (Q_n and Q_p) and the heat exchanged per carrier ($q|\Pi_n| - E_{Q,n}$ and $E_{Q,p} - q|\Pi_p|$) vs the bias in an InGaAs pn junction with doping levels $N_A = N_D = 2 \times 10^{19}\,\mathrm{cm}^{-3}$. According to the heat exchange performance, we can roughly divide these curves into three bias regimes: the forward heating regime, the reverse cooling regime, and the reverse heating regime. The band alignment and the associated energy levels are indicated in Fig. 3(c). When the junction is forward biased, with the increasing bias, Q_n and Q_p first increase and then drop to zero where the current density vanishes. This dependence of Q_n and Q_p on the bias is consistent with the associated current density. We also observe that the heating of the junction is asymmetric with Q_n being much larger than Q_p under the forward bias. The ratio Q_n/Q_p can be as large as 15. This can be verified by investigating the heat exchanged per carrier in Fig. 3(b), where $q|\Pi_n| - E_{Q,n}$ increases approximately linearly with the bias, while $E_{Q,p} - q|\Pi_p|$ is relatively unchanged. We explain this performance as follows. Under forward bias, the current is the net electron tunneling current from the n bulk to the p bulk. The filled states in the n bulk are approximately between E_c and $E_{F,n}$, and the empty states in the p bulk are between E_v and $E_{F,p}$. Since the difference between E_v and $E_{F,p}$ is much smaller than E_c and $E_{F,n}$ because of the existence of the heavy hole valence band (HH-VB), E_Q is pinned by the narrow energy window of the empty states near $E_{F,p}$ in the p bulk. Therefore, on the p side $E_{Q,p} - q|\Pi_p| \approx q|\Pi_p|$ is approximately a few kT. While on the n side, $q|\Pi_n| - E_{Q,n} \approx q|\Pi_n| - E_{F,p} \approx E_{F,n} - E_{F,p} = qV$.

When the junction is operated under small reverse bias, we can observe cooling on both sides of the junction. Specifically, Q_n and Q_p are negative under $V \approx -0.04$ to 0 V and $V \approx -0.05$ to 0 V, respectively. This phenomenon indicates that E_Q is between $E_{F,n} + q\Pi_n$ and $E_{F,p} + q\Pi_p$. The alignment of the energy levels is qualitatively depicted in the second plot of Fig. 3(c). The dependences of $|Q_n|$ and $|Q_p|$ on the bias are nonmonotonic with $|Q_n|$ and $|Q_p|$ approximately peaking at $V = -0.02$ V and $V = -0.025$ V, respectively. This is due to the fact that the current and the heat exchange per carrier have opposite trends with increasing reverse bias. As the reverse bias increases, the current increases, while the magnitude of

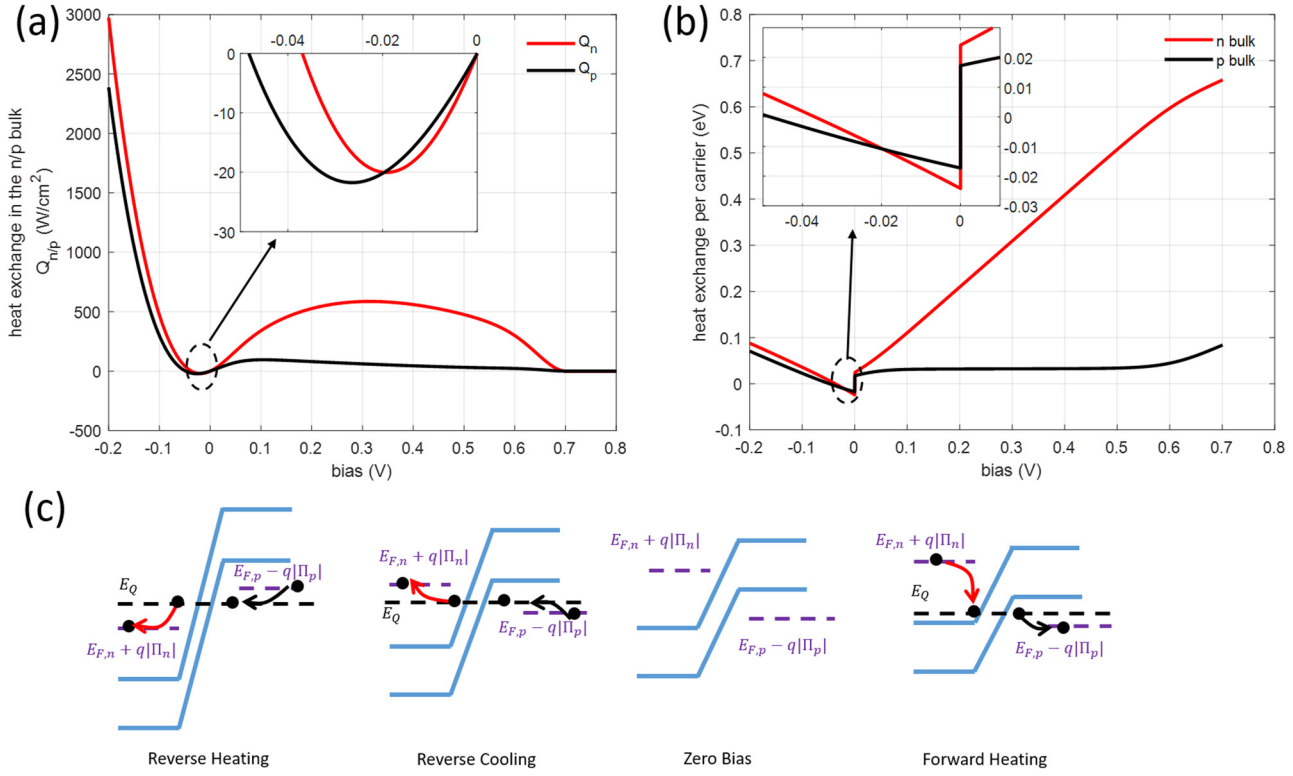

FIG. 3. (a) The heat exchange $Q_{n/p}$ in the n and p bulks of an InGaAs pn junction doped at $N_A = N_D = 2 \times 10^{19}\,\mathrm{cm}^{-3}$ vs the bias. The red lines and black lines indicate Q_n and Q_p, respectively. (b) The heating exchange per carrier $q|\Pi_n| - E_{Q,n}$ and $E_{Q,p} - q|\Pi_n|$ vs the bias in the n and p bulks. The red lines and black lines indicate the n and p bulks, respectively. Note that the lines are terminated when the associated current vanishes. (c) The alignment of the energy levels includes the transport energy in the bulk (purple dashed lines) and the averaged energy of the tunneling electrons (black dashed lines) in various bias regimes. The arrows indicate the current directions as well as the associated heat exchange. The blue solid lines indicate the band structures.

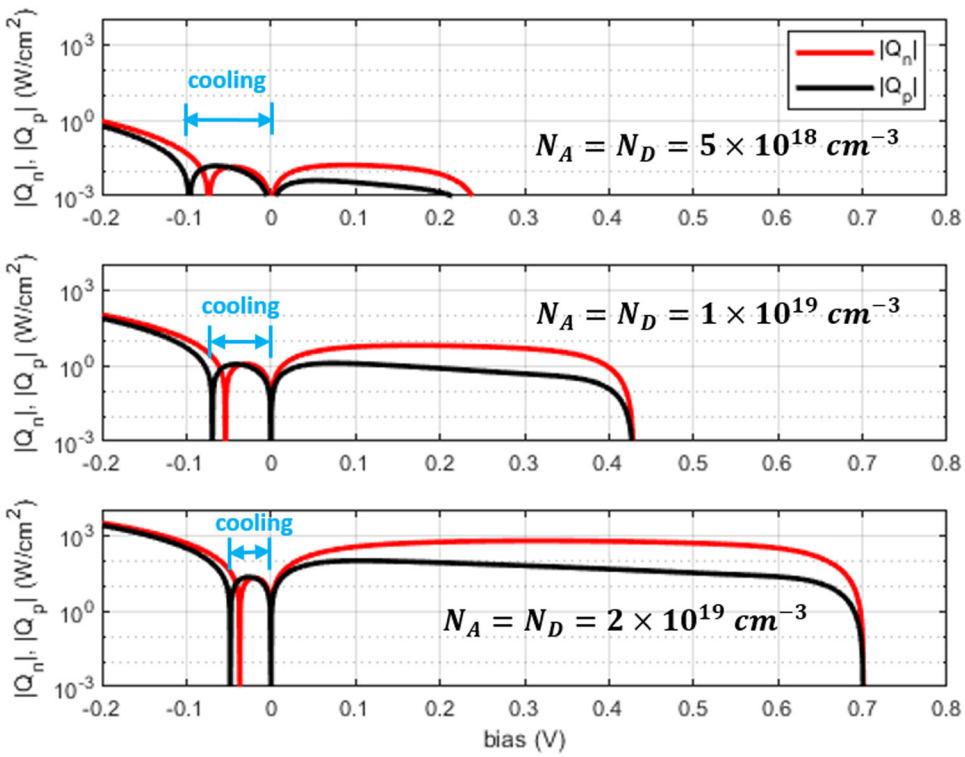

FIG. 4. The heat exchange $|Q_{n/p}|$ in the n and p bulks vs the bias with various doping levels. The red lines and black lines indicate $|Q_n|$ and $|Q_p|$, respectively. The reverse cooling regimes are label in the plots.

the heat exchange per carrier decreases. [Fig. 3(b)]. Note that the sign changing of the heat exchange per carrier at $V = 0$ is due to the change of the current direction. Also, note that, in this situation, heating happens at the semiconductor/contact interfaces.

Under larger negative bias $V < -0.05$ V, significant heating can be observed on both sides of the junction. The magnitudes of Q_n and Q_p are similar. In this situation, as depicted in the first plot of Fig. 3(c), E_Q is approximately in the middle of $E_{F,n} + q\Pi_n$ and $E_{F,p} + q\Pi_p$. Unlike the cooling regime, here the $E_{F,n} + q\Pi_n$ is lower than $E_{F,p} + q\Pi_p$ due to the large reverse bias.

We can further examine our assumption of the energy-independent relaxation time here. Under small reverse bias, cooling happens and the electrons absorb heat from the lattice [Fig. 3(a)]. This is associated with phonon absorption. Compared with acoustic phonon absorption, POP absorption is usually stronger in III-V materials, and the POP absorption relaxation time is approximately energy-independent.[48] Under large reverse bias, the heat exchange per carrier is usually higher than the POP emission threshold of 33 meV; hence, POP emission with an energy-independent relaxation time dominates energy relaxation [Fig. 3(b)]. Under forward bias, especially in the p bulk, the assumption can be problematic since the heat exchange per carrier is comparable to the POP emission energy threshold. The acoustic phonon scattering may have a significant contribution to energy relaxation in these situations.[47] However, as we pointed out above, the small integration windows in Eqs. (7a) and (7b) lead to weak dependence of $\Pi_{n/p}$ on r, and thus the approximation is still valid.

We conclude by presenting $|Q_n|$ and $|Q_p|$ of tunneling junctions with various doping levels in Fig. 4. The distinct three bias regimes can be observed and the associated heat exchange performance is consistent with our previous discussions. As the doping level increases, the magnitudes of heat exchange increase due to the larger current density. Also, the cooling regime shrinks because $|\Pi|$ decreases with doping.[20]

IV. INTERNAL TEMPERATURE PROFILES

In this section, we discuss the internal temperature profiles in the bulk regions of tunneling junctions. We use an InGaAs tunneling junction with a doping level of $N_A = N_D = 2 \times 10^{19}$ cm^{-3}. We consider $V = -0.2$ V, $V = -0.02$ V, and $V = 0.1$ V as the typical situations for reverse heating, reverse cooling, and forward heating, respectively. Q_n and Q_p are computed using Eq. (11). The distribution of Q_n is modeled as an exponential decaying function with energy relaxation length l_n in the n bulk. For the distribution of Q_p, as we discussed above, since l_p is much smaller than l_n, we assume that the heating in the p bulk is a δ-function in space, or effectively $l_p = 0$, for simplicity. Fourier's law is used to compute the temperature profile from the heat exchange. Two device structures are used in our simulation. One is with a long p substrate ($>200\,\mu$m) and short n bulk ($1\,\mu$m), which is a simplified thin film device. The other is with the n and p bulk of the same length of $1\,\mu$m. On both electrodes, we apply boundary conditions of a fixed temperature of $\Delta T = 0$.

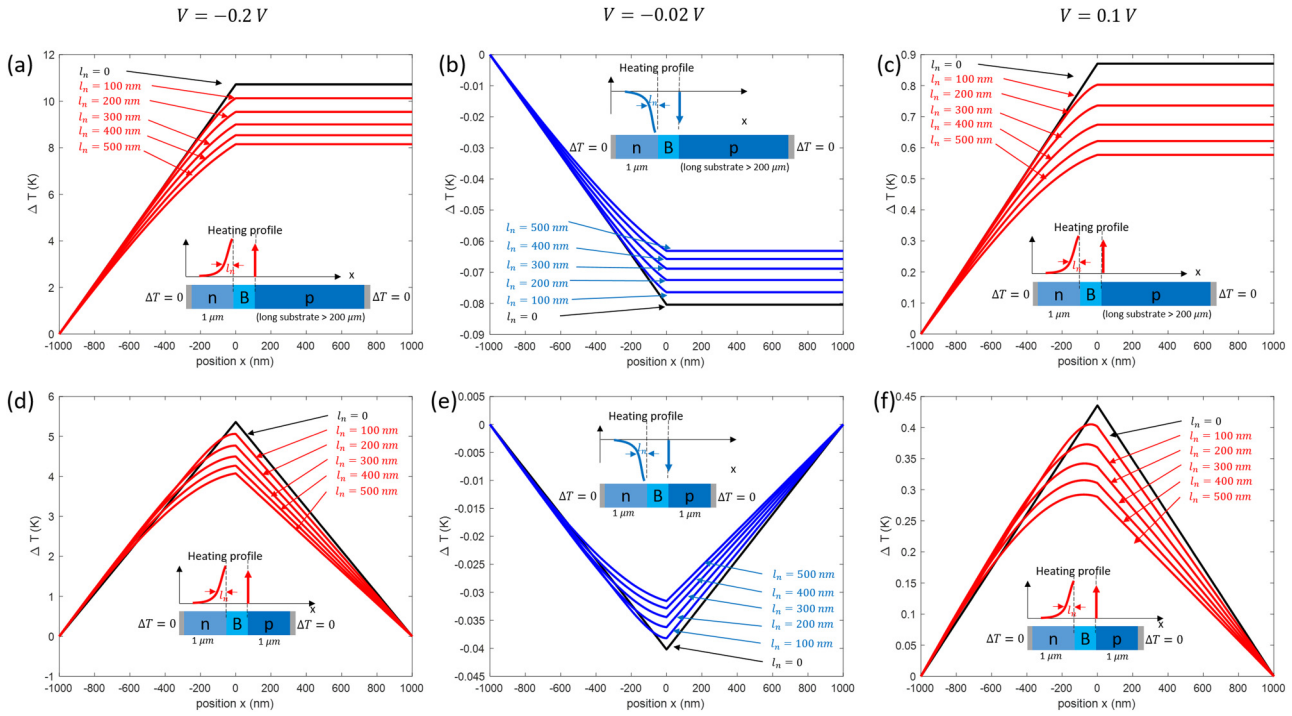

FIG. 5. Internal temperature profiles of tunneling junctions with various l_n, device structures, and operating bias. (a)–(c) Device structures with long p substrates. (d)–(f) Device structures with short n and p bulk. The operating bias are −0.2 V, −0.02 V, and 0.1 V in (a)–(d), (b)–(e), and (c)–(f), respectively. The inset plots indicate the structures and the heating profiles. The blocks labeled n and p indicate the neutral regions in the corresponding bulk. The blocks labeled with B indicate the barrier region.

In Fig. 5, we present the internal temperature profiles of the two device structures under various operating bias. ΔT is the difference of the internal temperature and the ambient temperature. Here, $x < 0$ and $x > 0$ indicate the n and p bulk, respectively. We vary $l_n = 0$–500 nm. Note that setting $l_n = 0$ is equivalent to assuming that the input power $J_{4b}V$ is dissipated entirely in the barrier region, which is similar to a simple resistor. In Figs. 5(a)–5(d), the junctions are biased in the reverse heating regime, where approximately half of the heat exchange is distributed in the n bulk. We observed the junction temperature with nonzero l_n to be lower than that from the resistor model. Given $l_n = 500$ nm, these deviations are approximately 2.5 K and 1.3 K for the structures with a long p bulk and a short p bulk, respectively. The relative deviations are both approximately 30%. In the forward heating regime [Figs. 5(c)–5(f)], as we mentioned, the heat exchange is more asymmetric with Q_n much larger than Q_p. Since Q_n contributes to the distributed heat exchange, the relative deviations in the forward heating regime, approximately 50%, are thus higher.

In the reverse cooling regime [Figs. 5(b)–5(e)], the temperature drop is on the order of several tens of mK. The temperature drop is higher with a long p substrate and a small l_n.

V. DISCUSSION AND CONCLUSION

In this letter, by using Kane's model with the four-band Hamiltonian, we compute the heat exchange in direct tunneling junctions and the associated internal temperature distributions. We observe three distinct bias regimes. In the forward heating regime, the heat exchange in the n bulk is much larger than that in the p bulk due to the pinning of the average tunneling electron energy. Considering this asymmetric nature of heat exchange and the distributed heating profile, we obtain lower junction temperatures compared with those from simple resistor models. In the reverse heating regime, the relative deviation is smaller because the heat exchange is less asymmetric. However, given that the current density can be high, the absolute deviations can be on the order of several K. Our model also predicts that when the reverse bias is small, cooling should be observed.

Our results suggest that the detailed heat exchange processes should be considered when designing devices with interband tunneling. For example, for TFETs that work under large reverse bias, one should compute the heat exchange in order to achieve better estimation of the junction temperature. As we present, using a simple resistor model can lead to approximately 30% deviations in our simulations.

A TFET can also work in the reverse cooling regime. Although the cooling phenomenon is a straightforward result of the Peltier effect, it is rarely mentioned in the related literature because the temperature drop is small. Recently, there are several new techniques reported that may be useful for such measurements. For example, by using scanning probe thermometry, sub-10 mK temperature resolution and nanoscale spatial resolution have been already

achieved.[21,49,50] The observations of the junction temperature drop in the reverse cooling regimes will not only verify our models but also have impact on the design of devices with interband tunneling.

Note that we only consider the heat exchange in the direct bandgap tunneling junctions in this work. A natural follow-on to this work would be to discuss heat exchange in indirect bandgap materials such as Si. The electron transport properties of indirect tunneling junctions have been investigated in Kane's original paper.[9,10] The Peltier coefficients of the n and p bulks can be computed through Eqs. (7a) and (7b) with a $\tau(E)$ associated with acoustic deformation phonons (ADPs) and intervalley scattering.[47] One also has to consider the heat exchange in the tunneling barrier region. Since the indirect band-to-band tunneling is usually assisted by phonons near the boundaries of the Brillouin zone, the heat exchange in the barrier should not be negligible. Semiclassical methods might not be applicable here because the thickness of a tunneling barrier is usually tens of nanometers and is much smaller than the phonon mean free path. Instead, a full quantum simulation, such as one with the NEGF formalism,[36] might be required.

REFERENCES

[1]C. Zener, Proc. R. Soc. Lond. A **145**, 523 (1934).
[2]L. Esaki, Phys. Rev. **109**, 603 (1958).
[3]A. Pethe, T. Krishnamohan, D. Kim, S. Oh, H.-S. P. Wong, and K. Saraswat, in *2006 16th Biennial University/Government/Industry Microelectronics Symposium* (IEEE, 2006), pp. 47–50.
[4]W. Anderson, Infrared Phys. **20**, 353 (1980).
[5]H. Mizuta and T. Tanoue, *The Physics and Applications of Resonant Tunnelling Diodes* (Cambridge University Press, 2006), Vol. 2.
[6]A. M. Ionescu and H. Riel, Nature **479**, 329 (2011).
[7]H. Lu and A. Seabaugh, IEEE J. Electron Devices Soc. **2**, 44 (2014).
[8]D. Sarkar, X. Xie, W. Liu, W. Cao, J. Kang, Y. Gong, S. Kraemer, P. M. Ajayan, and K. Banerjee, Nature **526**, 91 (2015).
[9]E. O. Kane, J. Phys. Chem. Solids **12**, 181 (1960).
[10]E. O. Kane, J. Appl. Phys. **32**, 83 (1961).
[11]L. Esaki, Science **183**, 1149 (1974).
[12]Z. Huang, T. Feuchtwang, P. Cutler, and E. Kazes, Phys. Rev. A **41**, 32 (1990).
[13]A. Schenk, Solid State Electron. **36**, 19 (1993).
[14]W.-S. Cho, M. Luisier, D. Mohata, S. Datta, D. Pawlik, S. L. Rommel, and G. Klimeck, Appl. Phys. Lett. **100**, 063504 (2012).
[15]A. Biswas, S. S. Dan, C. L. Royer, W. Grabinski, and A. M. Ionescu, Microelectron. Eng. **98**, 334 (2012),
[16]Q. Smets, D. Verreck, A. S. Verhulst, R. Rooyackers, C. Merckling, M. Van De Put, E. Simoen, W. Vandervorst, N. Collaert, V. Y. Thean, B. Sorée, G. Groeseneken, and M. M. Heyns, J. Appl. Phys. **115**, 184503 (2014).
[17]A. Pan and C. O. Chui, J. Appl. Phys. **116**, 054508 (2014).
[18]C.-H. Shih and N. Dang Chien, J. Appl. Phys. **115**, 044501 (2014).
[19]H. Carrillo-Nuñez, A. Ziegler, M. Luisier, and A. Schenk, J. Appl. Phys. **117**, 234501 (2015).
[20]K. P. Pipe, R. J. Ram, and A. Shakouri, Phys. Rev. B **66**, 125316 (2002).
[21]H.-K. Lyeo, A. A. Khajetoorians, L. Shi, K. P. Pipe, R. J. Ram, A. Shakouri, and C. K. Shih, Science **303**, 816 (2004).
[22]A. Shakouri, Annu. Rev. Mater. Res. **41**, 399 (2011).
[23]J. B. Xu, K. Läuger, R. Möller, K. Dransfeld, and I. H. Wilson, Appl. Phys. A **59**, 155 (1994).
[24]T. Fisher and D. Walker, J. Heat Transfer **124**, 954 (2002).
[25]I. Bat'ko and M. Bat'ková, Eur. Phys. J. Appl. Phys. **31**, 191 (2005).
[26]K. Maki and A. Griffin, Phys. Rev. Lett. **15**, 921 (1965).
[27]P. J. Koppinen and I. J. Maasilta, Phys. Rev. Lett. **102**, 165502 (2009).
[28]M. Walter, J. Walowski, V. Zbarsky, M. Münzenberg, M. Schäfers, D. Ebke, G. Reiss, A. Thomas, P. Peretzki, M. Seibt, J. S. Moodera, M. Czerner, M. Bachmann, and C. Heiliger, Nat. Mater. **10**, 742 (2011).
[29]J. Zhang, M. Bachman, M. Czerner, and C. Heiliger, Phys. Rev. Lett. **115**, 037203 (2015).
[30]W. Vandenberghe, B. Sorée, W. Magnus, and G. Groeseneken, J. Appl. Phys. **107**, 054520 (2010).
[31]A. Schenk, R. Rhyner, M. Luisier, and C. Bessire, in *2011 International Conference on Simulation of Semiconductor Processes and Devices* (IEEE, 2011), pp. 263–266.
[32]A. Di Carlo, P. Vogl, and W. Pötz, Phys. Rev. B **50**, 8358 (1994).
[33]K. Ganapathi and S. Salahuddin, J. Appl. Phys. **111**, 124506 (2012).
[34]J. B. Krieger, Ann. Phys. **36**, 1 (1966).
[35]A. Pan and C. O. Chui, J. Appl. Phys. **116**, 054509 (2014).
[36]R. Lake, G. Klimeck, R. C. Bowen, and D. Jovanovic, J. Appl. Phys. **81**, 7845 (1997).
[37]K. Louarn, Y. Claveau, D. Hapiuk, C. Fontaine, A. Arnoult, T. Taliercio, C. Licitra, F. Piquemal, A. Bounouh, N. Cavassilas, and G. Almuneau, J. Phys. D: Appl. Phys. **50**, 385109 (2017).
[38]M. Zebarjadi, A. Shakouri, and K. Esfarjani, Phys. Rev. B **74**, 195331 (2006).
[39]B. Moyzhes and V. Nemchinsky, Appl. Phys. Lett. **73**, 1895 (1998).
[40]S. Slipchenko, Z. Sokolova, N. Pikhtin, K. Borschev, D. Vinokurov, and I. Tarasov, Semiconductors **40**, 990 (2006).
[41]C.-Y. Tsai, C.-Y. Tsai, R. M. Spencer, Y.-H. Lo, and L. F. Eastman, IEEE J. Quantum Electron. **32**, 201 (1996).
[42]C.-Y. Tsai, C.-Y. Tsai, Y.-H. Lo, and L. Eastman, IEEE J. Quantum Electron. **31**, 2148 (1995).
[43]J. Wang and H. C. Schweizer, IEEE J. Quantum Electron. **33**, 1350 (1997).
[44]H. J. Goldsmid, *Electronic Refrigeration* (Pion, 1986).
[45]W. Nakwaski, Electron. Technol. **14**, 81 (1984).
[46]J. Tauc, *Photo and Thermoelectric Effects in Semiconductors* (Pergamon, 1962), Vol. 2.
[47]M. Lundstrom, *Fundamentals of Carrier Transport* (Cambridge University Press, 2009).
[48]T.-H. Liu, J. Zhou, B. Liao, D. J. Singh, and G. Chen, Phys. Rev. B **95**, 075206 (2017).
[49]F. Menges, P. Mensch, H. Schmid, H. Riel, A. Stemmer, and B. Gotsmann, Nat. Commun. **7**, 10874 (2016).
[50]K. Kim, W. Jeong, W. Lee, and P. Reddy, ACS Nano **6**, 4248 (2012).